

Mechanisms of Autoinhibition of IRF-7 and a Probable Model for Inactivation of IRF-7 by Kaposi's Sarcoma-associated Herpesvirus Protein ORF45^{*§}

Received for publication, June 5, 2010, and in revised form, October 8, 2010. Published, JBC Papers in Press, October 27, 2010, DOI 10.1074/jbc.M110.150920

Narayanan Sathish[‡], Fan Xiu Zhu[§], Ellis E. Golub[¶], Qiming Liang[§], and Yan Yuan^{‡1}

From the Departments of [‡]Microbiology and [¶]Biochemistry, University of Pennsylvania School of Dental Medicine, Philadelphia, Pennsylvania 19104 and the [§]Department of Biological Science, Florida State University, Tallahassee, Florida 32306

IRF-7 is the master regulator of type I interferon-dependent immune responses controlling both innate and adaptive immunity. Given the significance of IRF-7 in the induction of immune responses, many viruses have developed strategies to inhibit its activity to evade or antagonize host antiviral responses. We previously demonstrated that ORF45, a KSHV immediate-early protein as well as a tegument protein of virions, interacts with IRF-7 and inhibits virus-mediated type I interferon induction by blocking IRF-7 phosphorylation and nuclear translocation (Zhu, F. X., King, S. M., Smith, E. J., Levy, D. E., and Yuan, Y. (2002) *Proc. Natl. Acad. Sci. U.S.A.* 99, 5573–5578). In this report, we sought to reveal the mechanism underlying the ORF45-mediated inactivation of IRF-7. We found that ORF45 interacts with the inhibitory domain of IRF-7. The most striking feature in the IRF-7 inhibitory domain is two α -helices H3 and H4 that contain many hydrophobic residues and two β -sheets located between the helices that are also very hydrophobic. These hydrophobic subdomains mediate intramolecular interactions that keep the molecule in a closed (inactive) form. Mutagenesis studies confirm the contribution of the hydrophobic helices and sheets to the autoinhibition of IRF-7 in the absence of viral signal. The binding of ORF45 to the critical domain of IRF-7 leads to a hypothesis that ORF45 may maintain the IRF-7 molecule in the closed form and prevent it from being activated in response to viral infection.

Interferon regulatory factors (IRFs)² are presently a diverse family of transcription factors widely implicated in mechanisms involving both antiviral defense and immune regulation (1–4). Two closely related members within this family, namely IRF-3 and IRF-7, have been identified as the key regu-

lators mediating the induction of type I IFNs (α/β) following a viral infection (5–7). Type I IFNs thus elicited the trigger for the transcription of downstream antiviral effector proteins, which through pleiotropic effects target and inhibit distinct stages in the viral life cycle ultimately helping to relieve the host cell of the viral burden (8, 9).

IRF-7 has been known to be the master regulator of type I interferon-dependent immune responses. The role of IRF-7 in the type I IFN induction pathway was earlier assessed employing IRF-7 deficient mice (IRF-7^{-/-}) (10, 11). In mouse embryonic fibroblasts isolated from these mice, following experimental viral infection, levels of type I IFN induction was found to be severely impaired, compared with levels obtained with the IRF-3 deficient mice (IRF-3^{-/-}) (10, 11). More importantly, the IRF-7-deficient mice (IRF-7^{-/-}) were much more susceptible to viral infections compared with IRF-3-deficient mice (IRF-3^{-/-}), with the increased viral susceptibility of the former well correlating with appreciable decreases in serum IFN levels. Another newly identified facet of IRF-7 is its critical role in a novel pathway involving the robust induction of type I IFNs. In this pathway, the Toll-like receptor molecule, exemplified by the Toll-like receptor 9 subfamily, subsequent to activation, recruits an adaptor protein MyD88. This adaptor protein specifically interacts with and activates IRF-7 (12, 13), resulting in type I IFN elicitation. The robust induction of type I IFN production by Toll-like receptor 9 in plasmacytoid dendritic cells is entirely dependent on IRF-7, with the MyD88-IRF-7 pathway governing the induction of CD8⁺ T-cell responses. Thus, all elements of type I IFN responses, whether the systemic production of IFN in innate antiviral immunity or the local action of IFN from plasmacytoid dendritic cells in adaptive immunity, are under control of IRF-7 (10, 11).

Hence it is not surprising that many viruses specifically antagonize the effects of IRF-7 (14–18). In the case of Kaposi's sarcoma-associated herpesvirus (KSHV), our laboratory had earlier shown that a viral tegument (19) and an immediate-early (IE) (20) protein, ORF45, inhibits both the phosphorylation and the nuclear translocation of IRF-7 (21), both of which constitute the pivotal steps in its activation. In a more recent study, we further showed that through targeting IRF-7, ORF45 effectively antagonizes the host antiviral responses, thereby helping the virus to establish a successful primary infection of cells (22). Thus based on these significant findings, we were prompted to understand the mechanism under-

* This work was supported, in whole or in part, by National Institutes of Health Grants R01CA86839 (to Y. Y.) and R01DE016680 (to F. X. Z.).

§ The on-line version of this article (available at <http://www.jbc.org>) contains supplemental Figs. S1 and S2.

¹ To whom correspondence should be addressed: 240 S. 40th St., Philadelphia, PA 19104. Tel.: 215-573-7556; Fax: 215-898-8385; E-mail: yuan2@pobox.upenn.edu.

² The abbreviations used are: IRF, interferon regulatory factor; KSHV, Kaposi's sarcoma-associated herpesvirus; aa, amino acid(s); 3-AT, 3-amino-1,2,4-triazole; DBD, DNA-binding domain; ID, inhibitory domain; IAD, IRF activation domain; VAD, virus-activated domain; SRD, signal response domain; CAD, constitutive activation domain; NLS, nuclear localization sequence; Y2H, yeast two-hybrid; AD, activation domain; EGFP, enhanced green fluorescent protein.

lying inactivation of IRF-7 by ORF45. Toward this, we attempted to map the domain(s) on IRF-7 specifically binding with ORF45. Our result indicated that KSHV ORF45 specifically bound to a region on IRF-7 spanning aa 305–466. This region has been earlier identified as an inhibitory domain (ID) (23). Additional domains across the entire length of the protein include (i) an amino-terminal DNA-binding domain (DBD) (aa 1–146); (ii) constitutive activation domain (CAD) (aa 151–246); (iii) virus activation domain (VAD) (aa 278–305); and (iv) a second transactivation component localized to the C-terminal, called the signal response domain (SRD) (aa 468–503) (23).

Among these different domains, it has been hypothesized that in the absence of a virus signal, the ID through intramolecular interactions maintains IRF-7 as a “closed” structure efficiently masking the N-terminal DBD and transactivation domains and the C-terminal signal response domains, thereby preventing the downstream activation of IRF-7 (4, 23, 24, 26). A similar function of the ID has also been suggested for other IRFs including IRF-3 (27–29), IRF-4 (30, 31), and IRF-5 (32).

The structural features of the ID region of IRF-7 has thus far remained elusive due to the absence of a known crystal structure for this protein. Subsequent to the finding that KSHV ORF45 interacts with the IRF-7 ID, combined with the possibility that ID critically controls the activation of IRF-7, motivated us to gain possible insights into this interesting region. By using mutagenesis analyses, combined with a molecular modeling approach, we identified distinct areas within the IRF-7 ID, enriched with hydrophobic amino acids, which vitally contributed to maintaining the IRF-7 molecule in closed conformation controlling the switch to an active form in response to viral infection.

EXPERIMENTAL PROCEDURES

Cells—Human embryonic kidney (HEK) 293T cells were maintained in Dulbecco’s modified Eagle’s medium (DMEM) supplemented with 10% heat-inactivated fetal bovine serum (FBS) and antibiotics.

Plasmid Constructs—The prey plasmids for the yeast two-hybrid (Y2H) assay consisted of (i) PCR amplified full-length IRF-7 cloned into the pACT2 vector (pACT2-IRF-7) in-frame with the GAL4 activation domain (AD) of the vector (Table 1); (ii) PCR amplified different truncation segments of IRF-7 cloned into the pACT2 vector (Table 1); (iii) deletion mutants of IRF-7 (ID1–ID10 with sequential amino acid deletions across the IRF-7 ID; Table 1) in the pACT2 vector, generated with a PCR-based mutagenesis system, ExSite (Stratagene) using a pair of phosphorylated oligonucleotides in opposite directions employing the pACT2-IRF-7 as the template; and (iv) PCR amplified IRF-7 exons (1–10) cloned into the pACT2 vector (Table 1). The bait plasmid was comprised of either the full-length KSHV ORF45 sequence or the IRF-7 ID sequence (aa 283–466) cloned into the pAS2-1 vector in-frame with the GAL4 DBD of the vector (Table 1).

The IRF-7 expressing plasmids for the co-immunoprecipitation assay consisted of (i) the full-length IRF-7 cloned into a pCMV-2-Flag expression vector designated as the pCMV-2-Flag-IRF-7 (Table 1) or (ii) different deletion mutants of IRF-7

(ID1–ID10 with sequential amino acid deletions across the IRF-7 ID; Table 1) constructed as earlier described employing the PCR-based mutagenesis system with pCMV-2-Flag-IRF-7 as the template. The KSHV ORF45 expressing plasmid, pCR3.1-ORF45, was constructed by cloning the entire ORF45 sequence into the pCR3.1 vector (Table 1).

Yeast Two-hybrid (Y2H) Analysis—Interaction abilities of (i) IRF-7 full-length and the respective truncation/deletion “prey” plasmids (Table 1) with KSHV ORF45 “bait” plasmid or (ii) IRF-7 exon (1–10) prey plasmids (Table 1) with IRF-7 ID bait plasmid were tested by an Y2H analysis, performed with the Matchmaker system (Clontech). Yeast strain Y190 was co-transformed with the respective prey and bait plasmids using lithium acetate. Yeast transformants positive for the prey-bait interaction were selected on plates lacking leucine, tryptophan, and histidine titrated against increasing concentrations (10–50 mM) of 3-amino-1,2,4-triazole (3-AT) and subsequently assayed for β -galactosidase activity using the standard colony-filter assay as described earlier (33). Thus interactions between the prey and bait were scored as positive only if there was activation of both the reporter genes, *HIS3* (growth on 3-AT incorporated plates lacking histidine) and *LacZ* (positive β -galactosidase assay).

Co-immunoprecipitation Assay and Immunoblotting—Subconfluent monolayers of HEK 293T cells were co-transfected with either the pCMV-2-Flag-IRF-7 (full-length) or the respective pCMV-2-Flag-IRF-7 deletion mutants (ID1–ID10) (Table 1), along with the ORF45 expressing plasmid (pCR3.1-ORF45) by the calcium-phosphate transfection method. Forty-eight hours post-transfection, cell monolayers were washed twice with ice-cold PBS followed by lysis with ice-cold lysis buffer (33). Cell lysates thus prepared were homogenized and clarified by high-speed centrifugation at 4 °C and subjected to an immunoprecipitation with an anti-FLAG M2-affinity gel (Sigma). Immunoprecipitated complexes were thoroughly washed with cold lysis buffer, resuspended in SDS-PAGE loading buffer, boiled for 10 min, and loaded onto SDS-PAGE gels (Invitrogen), and subsequently immunoblotted with a rabbit polyclonal anti-ORF45 antibody to detect the presence of co-precipitating ORF45.

Luciferase Assay—The promoter sequences of human IFNA1 (–140 to +9) and IFNB (–280 to +20) were cloned into the pGL3-basic vector (Promega). Subconfluent HEK 293T cells grown in 24-well plates were transfected with 20 ng of pRL-TK reporter (*Renilla* luciferase as an internal control), 200 ng of pGL-3 reporter (firefly luciferase, experimental reporter), and 40 ng of IRF-7 expressing plasmid (IRF-7 full-length) or the IRF-7 ID deletion mutants, ID1–ID20, cloned into a pCMV-2-FLAG vector; Table 1) employing the Qiagen Effectene transfection kit. At 8 h post-transfection, 80 hemagglutinin units (HA) of Sendai virus were added to one set of transfected cells. Twenty-four hours post-transfection, cell lysates were collected and a luciferase assay was performed with the Dual-luciferase assay kit from Promega (Madison, WI).

Immunofluorescence Assay—The full-length and the different IRF-7 ID deletion mutants, ID10–ID20, cloned into a pEGFP-C3 vector (Clontech) (Table 1) that allows for expression of these

Mechanisms of Inhibition of IRF-7

TABLE 1
Characteristics of plasmids employed in different assays in this study

Vector or plasmid	Construct	Characteristics
Yeast two-hybrid		
Prey plasmids		
IRF-7 full-length	pACT2-IRF-7	IRF-7 full-length (aa 1–503) cloned in pACT2
IRF-7 truncation mutants	pACT2-IRF-7 (77–503) pACT2-IRF-7 (92–503) pACT2-IRF-7 (181–503) pACT2-IRF-7 (255–503) pACT2-IRF-7 (283–503) pACT2-IRF-7 (305–503) pACT2-IRF-7 (255–413) pACT2-IRF-7 (283–452) pACT2-IRF-7 (283–466) pACT2-IRF-7 (283–490)	IRF-7 segment spanning aa 77–503 cloned in pACT2 IRF-7 segment spanning aa 92–503 cloned in pACT2 IRF-7 segment spanning aa 181–503 cloned in pACT2 IRF-7 segment spanning aa 255–503 cloned in pACT2 IRF-7 segment spanning aa 283–503 cloned in pACT2 IRF-7 segment spanning aa 305–503 cloned in pACT2 IRF-7 segment spanning aa 255–413 cloned in pACT2 IRF-7 segment spanning aa 283–452 cloned in pACT2 IRF-7 segment spanning aa 283–466 cloned in pACT2 IRF-7 segment spanning aa 283–490 cloned in pACT2
IRF-7 deletion mutants	pACT2-ID1 (Δ 283–304) ^a pACT2-ID2 (Δ 305–321) pACT2-ID3 (Δ 322–341) pACT2-ID4 (Δ 342–361) pACT2-ID5 (Δ 362–382) pACT2-ID6 (Δ 383–403) pACT2-ID7 (Δ 404–423) pACT2-ID8 (Δ 424–445) pACT2-ID9 (Δ 446–466) pACT2-ID10 (Δ 283–466)	IRF-7 ID (aa spanning 283–304) deleted from pACT2-IRF-7 IRF-7 ID (aa spanning 305–321) deleted from pACT2-IRF-7 IRF-7 ID (aa spanning 322–341) deleted from pACT2-IRF-7 IRF-7 ID (aa spanning 342–361) deleted from pACT2-IRF-7 IRF-7 ID (aa spanning 362–382) deleted from pACT2-IRF-7 IRF-7 ID (aa spanning 383–403) deleted from pACT2-IRF-7 IRF-7 ID (aa spanning 404–423) deleted from pACT2-IRF-7 IRF-7 ID (aa spanning 424–445) deleted from pACT2-IRF-7 IRF-7 ID (aa spanning 446–466) deleted from pACT2-IRF-7 IRF-7 ID (aa spanning 283–466) deleted from pACT2-IRF-7
IRF-7 exons	pACT2-IRF-7-exon 1/2 pACT2-IRF-7-exon 3 pACT2-IRF-7-exon 3 pACT2-IRF-7-exon 4 pACT2-IRF-7-exon 5 pACT2-IRF-7-exon 6 pACT2-IRF-7-exon 7 pACT2-IRF-7-exon 8 pACT2-IRF-7-exon 9 pACT2-IRF-7-exon 10	IRF-7 exon 1–61 cloned in pACT2 IRF-7 exon 3 spanning aa 62–132 cloned in pACT2 IRF-7 exon 3 spanning aa 62–132 cloned in pACT2 IRF-7 exon 4 spanning aa 133–152 cloned in pACT2 IRF-7 exon 5 spanning aa 153–227 cloned in pACT2 IRF-7 exon 6 spanning aa 228–256 cloned in pACT2 IRF-7 exon 7 spanning aa 257–283 cloned in pACT2 IRF-7 exon 8 spanning aa 283–413 cloned in pACT2 IRF-7 exon 9 spanning aa 413–452 cloned in pACT2 IRF-7 exon 10 spanning aa 452–503 cloned in pACT2
Bait plasmids	pAS2–1-ORF45 pAS2–1-IRF-7-ID	KSHV ORF45 full length (aa 1–407) cloned in pAS2–1 IRF-7 ID spanning aa 283–466 cloned in pAS2–1
Co-immunoprecipitation		
IRF-7 expressing plasmids	pCMV-2-Flag-IRF-7 pCMV-2-Flag-ID1 (Δ 283–304) pCMV-2-Flag-ID2 (Δ 305–321) pCMV-2-Flag-ID3 (Δ 322–341) pCMV-2-Flag-ID4 (Δ 342–361) pCMV-2-Flag-ID5 (Δ 362–382) pCMV-2-Flag-ID6 (Δ 383–403) pCMV-2-Flag-ID7 (Δ 404–423) pCMV-2-Flag-ID8 (Δ 424–445) pCMV-2-Flag-ID9 (Δ 446–466) pCMV-2-Flag-ID10 (Δ 283–466)	IRF-7 full-length (aa 1–503) cloned in pCMV-2-Flag IRF-7 ID (aa spanning 283–304) deleted from pCMV-2-Flag-IRF-7 IRF-7 ID (spanning aa 305–321) deleted from pCMV-2-Flag-IRF-7 IRF-7 ID (spanning aa 322–341) deleted from pCMV-2-Flag-IRF-7 IRF-7 ID (spanning aa 342–361) deleted from pCMV-2-Flag-IRF-7 IRF-7 ID (spanning aa 362–382) deleted from pCMV-2-Flag-IRF-7 IRF-7 ID (spanning aa 383–403) deleted from pCMV-2-Flag-IRF-7 IRF-7 ID (spanning aa 404–423) deleted from pCMV-2-Flag-IRF-7 IRF-7 ID (spanning aa 424–445) deleted from pCMV-2-Flag-IRF-7 IRF-7 ID (spanning aa 446–466) deleted from pCMV-2-Flag-IRF-7 IRF-7 ID (spanning aa 283–466) deleted from pCMV-2-Flag-IRF-7
ORF45 expressing plasmid	pCR3.1-ORF45	KSHV ORF45 full length (aa 1–407) cloned in pCR3.1 vector
Luciferase reporter assays		
IRF-7 expressing plasmids	pCMV-2-Flag-IRF-7 (and) pCMV-2-Flag-ID1-ID10 pCMV-2-Flag-ID11 (Δ 283–452) pCMV-2-Flag-ID12 (Δ 283–445) pCMV-2-Flag-ID13 (Δ 283–423) pCMV-2-Flag-ID14 (Δ 283–412) pCMV-2-Flag-ID15 (Δ 283–403) pCMV-2-Flag-ID16 (Δ 283–382) pCMV-2-Flag-ID17 (Δ 283–361) pCMV-2-Flag-ID18 (Δ 283–341) pCMV-2-Flag-ID19 (Δ 283–321) pCMV-2-Flag-ID20 (Δ 283–304)	Same plasmids as above IRF-7 ID (aa spanning 283–452) deleted from pCMV-2-Flag-IRF-7 IRF-7 ID (aa spanning 283–445) deleted from pCMV-2-Flag-IRF-7 IRF-7 ID (aa spanning 283–423) deleted from pCMV-2-Flag-IRF-7 IRF-7 ID (aa spanning 283–412) deleted from pCMV-2-Flag-IRF-7 IRF-7 ID (aa spanning 283–403) deleted from pCMV-2-Flag-IRF-7 IRF-7 ID (aa spanning 283–382) deleted from pCMV-2-Flag-IRF-7 IRF-7 ID (aa spanning 283–361) deleted from pCMV-2-Flag-IRF-7 IRF-7 ID (aa spanning 283–341) deleted from pCMV-2-Flag-IRF-7 IRF-7 ID (aa spanning 283–321) deleted from pCMV-2-Flag-IRF-7 IRF-7 ID (aa spanning 283–304) deleted from pCMV-2-Flag-IRF-7
Immunofluorescence assays		
IRF-7 expressing plasmids	pEGFP-C3-IRF-7 pEGFP-C3-ID10 (Δ 283–466) pEGFP-C3-ID11 (Δ 283–452) pEGFP-C3-ID12 (Δ 283–445) pEGFP-C3-ID13 (Δ 283–423) pEGFP-C3-ID14 (Δ 283–412) pEGFP-C3-ID15 (Δ 283–403) pEGFP-C3-ID16 (Δ 283–382) pEGFP-C3-ID17 (Δ 283–361) pEGFP-C3-ID18 (Δ 283–341) pEGFP-C3-ID19 (Δ 283–321) pEGFP-C3-ID20 (Δ 283–304)	IRF-7 full-length (aa 1–503) cloned in pEGFP-C3 IRF-7 ID (aa spanning 283–466) deleted from pEGFP-C3-IRF-7 IRF-7 ID (aa spanning 283–452) deleted from pEGFP-C3-IRF-7 IRF-7 ID (aa spanning 283–445) deleted from pEGFP-C3-IRF-7 IRF-7 ID (aa spanning 283–423) deleted from pEGFP-C3-IRF-7 IRF-7 ID (aa spanning 283–412) deleted from pEGFP-C3-IRF-7 IRF-7 ID (aa spanning 283–403) deleted from pEGFP-C3-IRF-7 IRF-7 ID (aa spanning 283–382) deleted from pEGFP-C3-IRF-7 IRF-7 ID (aa spanning 283–361) deleted from pEGFP-C3-IRF-7 IRF-7 ID (aa spanning 283–341) deleted from pEGFP-C3-IRF-7 IRF-7 ID (aa spanning 283–321) deleted from pEGFP-C3-IRF-7 IRF-7 ID (aa spanning 283–304) deleted from pEGFP-C3-IRF-7

^a Δ denotes deletion of the indicated amino acid region (represented within parentheses).

proteins as fusions to the C terminus of EGFP were constructed. HEK 293T cells grown on coverslips were transfected with the above plasmids employing the Qiagen Effectene transfection kit. For virus infection, the transfected cells were challenged with Sendai virus (80 hemagglutinin units/ml) at 16 h post-transfec-

tion. Twelve hours post-infection, both the uninfected and the virus-infected cells were washed with PBS and subsequently fixed. The coverslips were mounted onto slides and examined under a confocal microscope (Nikon) and images were processed with a LaserSharp 2000 software.

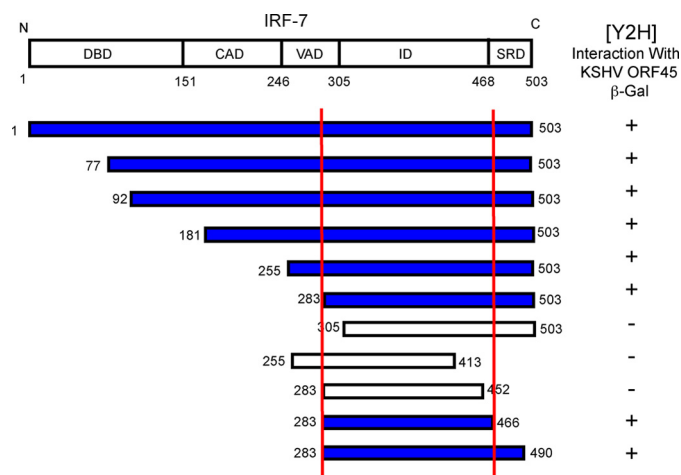


FIGURE 1. KSHV ORF45 binds to a specific region on IRF-7 encompassing amino acids 283–466. The full-length IRF-7 and a series of truncation mutants across the entire length of IRF-7 cloned into the pACT2 vector (prey) were individually co-transformed along with the full-length ORF45 in the pAS2-1 vector (bait) into yeast strain Y190. Yeast transformants positive for the prey-bait interaction were selected on plates lacking leucine, tryptophan, and histidine titrated against increasing concentrations (10–50 mM) of 3-AT and subsequently assayed for β -galactosidase activity (standard colony filter assay), the findings of which are represented on the right of each prey construct. *Dark blue rectangles* indicate the IRF-7 prey plasmids that interact with KSHV ORF45, whereas the *white open rectangles* indicate IRF-7 constructs that lost their ability to interact with the latter. The numbers on the side of the rectangles indicate the corresponding amino acid position. The region in IRF-7 identified as being sufficient for its interaction with KSHV ORF45 is enclosed within the red lines. The upper panel depicts a schematic representation of the domain structure of IRF-7 with the N-terminal DBD followed by the CAD and the VAD. The C-terminal half of IRF-7 is constituted by the ID and SRD. The numbers below this representation indicate the corresponding amino acid positions of the respective domains.

Molecular Modeling—The x-ray crystal structure of IRF-3 (Protein Data Bank 1J2F) was obtained from the Protein Data Bank at the Research Collaboratory for Structural Bioinformatics. The C-terminal section of the B chain (residues 189–422) served as the structure template. The sequence of IRF-7 (residues 281–503) was aligned to the IRF-3 structure by sequence similarity, and the coordinates of homologous amino acids were transferred from IRF-3 to IRF-7 using the Homology module of Insight II (Accelrys). The coordinates of unassigned residues of IRF-7 were estimated by standard interpolation methods. The final structure was then subjected to energy minimization using the Discover module of Insight II.

RESULTS AND DISCUSSION

KSHV ORF45 Binds to a Specific Region on IRF-7 Encompassing Amino Acids 283–466—Earlier findings from our laboratory revealed that KSHV ORF45 inhibited IRF-7 activation (21) thus effectively antagonizing the host antiviral immune responses, helping to establish a successful primary viral infection (22). Thus toward further comprehending the interaction dynamics between IRF-7 and ORF45, we attempted to map the region(s) on IRF-7 interacting with ORF45. The full-length IRF-7 and a series of truncation mutants across the entire length of the protein (Fig. 1) cloned into the pACT2 vector (prey) were co-transformed along with full-length ORF45 in pAS2-1 vector (bait) into yeast strain Y190. This allowed for the simultaneous expression of both the prey and bait proteins within the yeast cells. Potential yeast transfor-

mants positive for prey-bait interactions were selected based on their *His⁺LacZ⁺* phenotype as indicated by their ability to grow on plates incorporated with 3-AT but lacking histidine (*His⁺*) with concomitant β -galactosidase (*LacZ*) activity.

The Y2H results indicated that full-length IRF-7 and mutants with successive truncations of the N terminus up to amino acid 283 (inclusive of mutants spanning amino acids 77–503, 92–503, 181–503, 255–503, and 283–503) were able to interact with KSHV ORF45 (Fig. 1) with comparable intensities (data not shown). However, any further truncation of the N terminus of IRF-7 beyond amino acid 283 failed to associate with ORF45 as seen with the mutant encompassing aa 305–503 (Fig. 1). On the other hand, a series of truncations from the C terminus of IRF-7 up to amino acid 466 (mutants spanning amino acids 283–490, 283–466) did not seem to affect the ability of IRF-7 to bind with ORF45. Binding was totally lost upon C-terminal truncations beyond amino acid 466 as exemplified by the mutant spanning IRF-7 aa 283–452 (Fig. 1). A fragment of IRF-7 encompassing aa 283–466 completely retained the ability to associate with ORF45 (Fig. 1). Taken together the Y2H study clearly indicated that KSHV ORF45 specifically binds to a region on IRF-7 encompassing aa 283–466.

The Entire ID of IRF-7 Is Necessary for Binding with KSHV ORF45—After mapping the ORF45-binding region on IRF-7 to the stretch spanning aa 283–466, we wanted to further dissect this region to investigate if ORF45 bound to designated stretches of amino acids within this region. We constructed a series of small deletion mutants of IRF-7, designated as mutants ID1–ID10, across the entire region spanning aa 283–466 as illustrated in Fig. 2A. The respective deletion mutants or the full-length IRF-7 that constituted the prey array were cotransformed into yeast cells along with the bait (ORF45 in pAS2-1 vector). *His⁺LacZ⁺* yeast transformants were subsequently selected as earlier described. In addition to its interaction with the full-length IRF-7, KSHV ORF45 also interacted with the IRF-7 deletion mutant ID1, which had a deletion of an amino acid stretch from 283 to 304 (Fig. 2A). However, ORF45 failed to interact with deletion mutant ID10, which completely lacked the IRF-7 aa stretch 283–466 and deletion mutants ID2–ID9, which harbored deletions of consecutive 20-amino acid stretches starting from the N terminus at aa 305 (Fig. 2A). Thus the Y2H result clearly indicated that ORF45 recognizes the entire sequence of IRF-7 within the stretch spanning amino acids 305–466.

To confirm these Y2H findings, we proceeded with a co-immunoprecipitation assay. The full-length IRF-7 or the respective IRF-7 deletion mutants, ID1–ID10, cloned into a FLAG-tagged expression vector were co-transfected along with an ORF45 expression vector (pCR3.1-ORF45) into subconfluent monolayers of HEK 293T cells. Forty-eight hours post-transfection, cells were lysed and the optimal and stable expression of both the co-transfected protein pairs was confirmed by immunoblotting employing specific anti-FLAG (Fig. 2B) and anti-ORF45 polyclonal antibodies, respectively (data not shown). Cell lysates immunoprecipitated with an anti-FLAG antibody-agarose affinity gel (Sigma) were sub-

Mechanisms of Inhibition of IRF-7

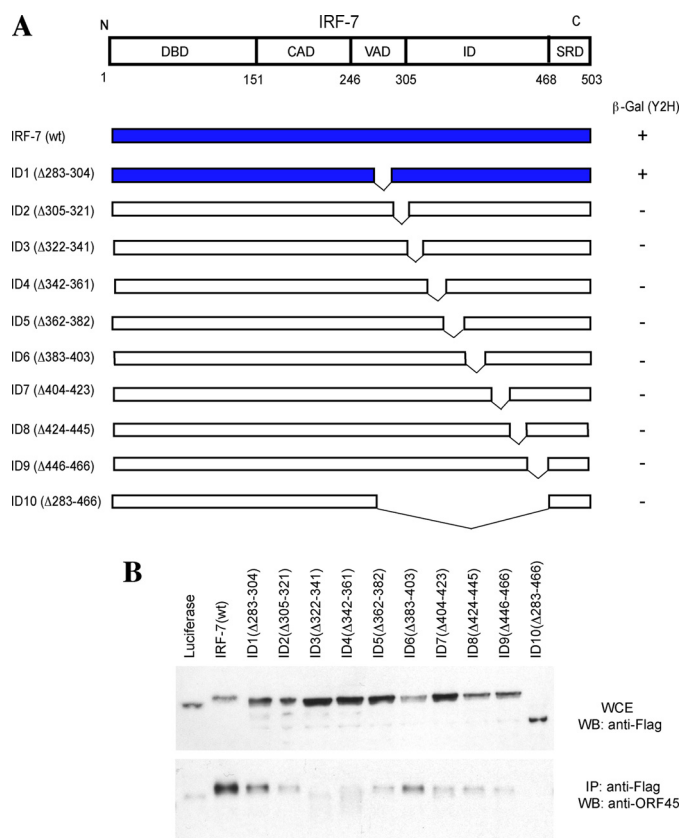


FIGURE 2. The entire ID of IRF-7 is required for binding with KSHV ORF45. *A*, the full-length and a series of small deletion mutants (ID1–ID10) of IRF-7 cloned into the pACT2 vector (prey) were individually co-transfected along with the full-length ORF45 in the pAS2-1 vector (bait) into yeast strain Y190. Yeast transformants positive for the prey-bait interaction were selected on plates lacking leucine, tryptophan, and histidine titrated against increasing concentrations (10–50 mM) of 3-AT and subsequently assayed for β -galactosidase activity (standard colony filter assay), the findings of represented on the *right* of each prey construct. *B*, subconfluent monolayers of HEK 293T cells were co-transfected with either the pCMV-2-Flag-IRF-7 (full-length) or the respective pCMV-2-Flag-IRF-7 deletion mutants (ID1–ID10) along with the ORF45 expressing plasmid (pCR3.1-ORF45). Expression levels of the IRF-7 full-length/deletion mutants in whole cell extracts (WCE) as detected by a Western blot (WB) employing anti-FLAG antibody is shown in the *upper panel*. The cell extracts were immunoprecipitated (IP) with an anti-FLAG antibody and the immunoprecipitates were resolved on SDS-PAGE gels and subjected to a Western blot with an anti-ORF45 antibody to detect levels of co-precipitating ORF45 (*lower panel*).

ected to Western blot to detect the presence of co-precipitating ORF45 employing a specific polyclonal antibody toward it.

ORF45 in addition to being immunoprecipitated with full-length IRF-7 was also efficiently precipitated with the IRF-7 mutant ID1 (aa Δ 283–304) (Fig. 2*B*). However, ORF45 failed to interact with all the other deletion mutants inclusive of mutant ID10 that completely lacked the stretch spanning aa 283–466 as evidenced by a barely detectable co-precipitation of ORF45 with these mutants compared with levels obtained with the full-length IRF-7 (Fig. 2*B*). Thus in essence the co-immunoprecipitation assay mirrored the findings of Y2H. The region on IRF-7, spanning amino acids 305–466, which specifically binds ORF45 (Fig. 2), has been recognized as the ID (23, 24).

Removal of the Entire ID from IRF-7 Leads to a Constitutive and Hyperactive Molecule but Any Small Deletions in the ID Results in Complete Loss of IRF-7 Transactivation—In perfect agreement with previous observations, we found that deletion

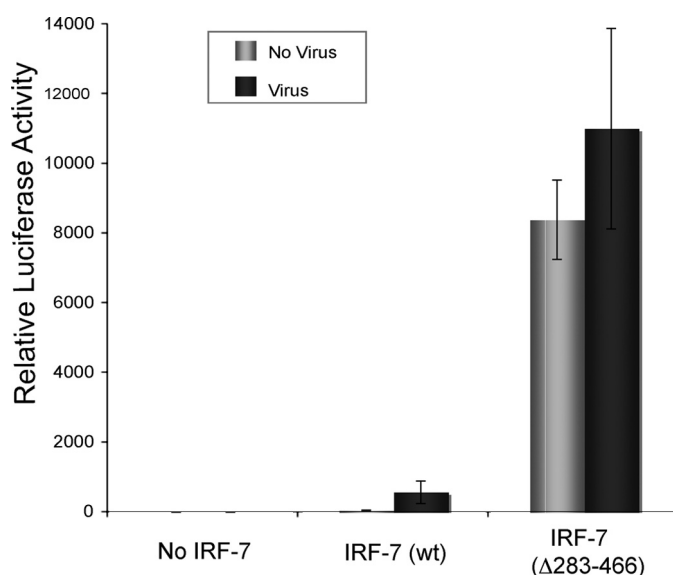


FIGURE 3. Deletion of the IRF-7 ID results in a constitutive and a hyperactive form of IRF-7. Reporter plasmids containing the firefly luciferase gene under control of the human IFNA1 promoter were co-transfected into subconfluent monolayers of HEK 293T cells along with either the wild-type (WT) IRF-7 or the ID-deleted form of IRF-7 (Δ 283–466). pRL-TK reporter plasmid encoding the *Renilla* luciferase was included as an internal control. At 8 h post-transfection, cells were either left uninfected (*black bars*) or infected with Sendai virus (*gray bars*). Cells were lysed and the luciferase (*Luc*) activities measured at 24 h post-infection and represented relative to the *Renilla* luciferase internal control gene.

of the above ORF45-binding region from IRF-7 generated a constitutive and hyperactive form of the protein in our study. This was convincingly illustrated by the potency of this mutant (IRF-7 ID aa Δ 283–466) in drastically activating the transcription of the IFNA1 promoter compared with the wild-type IRF-7 irrespective of challenge by Sendai virus (Fig. 3). This finding credibly demonstrates that the ID of IRF-7 plays a critical role in maintaining the protein in a latent/inactive state making it strikingly less amenable toward the activation of the IFN promoters. Thus given the fact that ID appears to silence IRF-7 transcription activity, the ID targeting ability of ORF45 clearly assumes significance. Interestingly, the ID of IRF-7 also seems to be targeted by other herpesviral proteins that contribute to host immune evasion including the EBV LF2 (14) and the KSHV vIRF-3 (15).

We next examined for the effects of small deletions in the ID region of IRF-7 on its transactivation ability. A reporter construct in which a luciferase gene is controlled by a human IFNA1 promoter was cotransfected into 293T cells together with the expression plasmids of wild-type IRF-7 or its respective small deletion mutants (ID1–ID9). The activity of the IFNA1 promoter in cells was enhanced up to 4-fold by expressing IRF-7. Sendai virus infection further stimulated the promoter by an additional 22-fold. However, the virus-induced transcription of the IFNA1 promoter was totally lost in all nine of the small internal deletion mutants, ID1–ID9 (Fig. 4), suggesting that any small deletion in the ID results in a deadlock of the IRF-7 molecule in an inactive form.

Structure and Function of ORF45-binding Region of IRF-7—Subsequent to observations that KSHV ORF45 specifically binds to the ID region on IRF-7 and that deletion of ID results

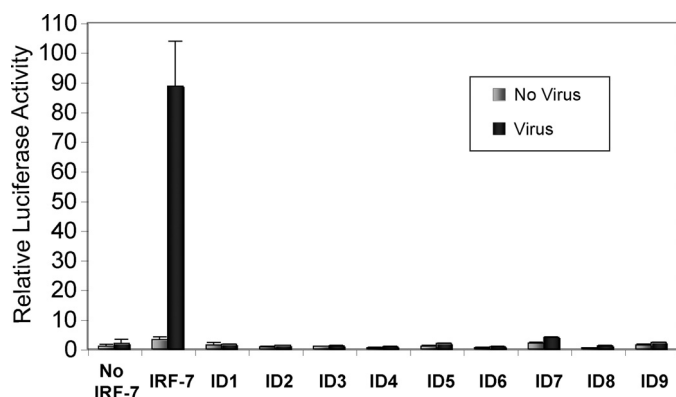


FIGURE 4. Any small deletions in the IRF-7 ID results in a complete loss of IRF-7 transactivation. Reporter plasmids containing the firefly luciferase gene under control of the human IFNA1 promoter were co-transfected into subconfluent monolayers of HEK 293T cells along with either the wild-type (WT) IRF-7 or the respective small deletion mutants of IRF-7 across the ID region. pRL-TK reporter plasmid encoding the *Renilla* luciferase was included as an internal control. At 8 h post-transfection, cells were either left uninfected (black bars) or infected with Sendai virus (gray bars). Cells were lysed and the luciferase (*Luc*) activities were measured at 24 h post-infection and are represented relative to the *Renilla* luciferase internal control gene.

in a constitutive and hyperactive form of IRF-7, we became motivated to learn further about the structural and functional characteristics of this important but less characterized region of IRF-7. To this end, it becomes desirable to solve the crystal structure of IRF-7 in its entirety or at least the C terminus IRF activation domains (IAD), which includes the virus-activated domain (VAD) (aa 246–305), ID (aa 305–466), and the SRD (aa 468–503) of the protein (23). However, despite repeated approaches by us, due to an insolubility problem, neither the entire IRF-7 nor its IAD fragment could be purified in a large quantity for its structural study by crystallography.

The crystal structure of IRF-3 (more specifically its C-terminal IRF activation domain or IAD) has been published (29, 34). A sequence alignment of IRF-3 and the IRF-7 (performed by GAP, Wisconsin Package (Accelrys) using specific algorithms (35, 36)) revealed conserved IAD between these two molecules with the overall fold almost being identical (Fig. 5A). The only difference pertaining to occurrence of protein secondary structures (37) in IRF-7 IAD was the absence of β -sheets, S3 and S4, in comparison to IRF-3 (29) with the occurrence and positioning of the remaining β -sheets and α -helices almost identical in both. Thus to maintain uniformity, we have applied the protein secondary structure numbering system of IRF-3 (29) to IRF-7 with β -sheets 3 and 4 as the only exclusion (Fig. 5A).

As is evident from Fig. 5A, the most striking feature of the IRF-7 IAD sequence is the preponderance of several hydrophobic amino acid-rich stretches. This includes (i) α -helices H3 and H4 in the ID region with Phe⁴⁰⁷, Val⁴⁰⁹, Phe⁴¹⁰, Phe⁴¹¹, Leu⁴¹⁴, Val⁴¹⁵, Phe⁴¹⁷, and Ala⁴¹⁹ in the H3 helix, and Leu⁴⁵⁷, Cys⁴⁵⁸, Val⁴⁶⁰, Leu⁴⁶², and Tyr⁴⁶⁵ in the H4 helix; (ii) β sheets (S10 and S11) located between H3 and H4 helices with Tyr⁴³¹, Leu⁴³², and Phe⁴³⁴ in the S10 sheet and Leu⁴⁴⁸, Val⁴⁴⁹, Leu⁴⁵⁰, Val⁴⁵¹, and Leu⁴⁵³ in the S11 sheet; and (iii) H5 α -helix in the C-terminal SRD with Ile⁴⁹², Phe⁴⁹⁵, Leu⁴⁹⁶, Met⁴⁹⁷, and Leu⁴⁹⁹. We believe that the increased hydropho-

bicity associated with the IRF-7 IAD could explain the insolubility of this component.

Due to the similarity in the overall fold of the IAD between IRF-3 and IRF-7, we were able to use protein structure modeling to predict the structure of the IRF-7 IAD employing the IRF-3 IAD structure as a template. Following sequence alignment of the IADs of IRF-3 (aa residues 189–422) with IRF-7 (aa 281–503), the coordinates of homologous amino acids were transferred from IRF-3 to IRF-7 using the Homology module of Insight II (Accelrys). Subsequently the coordinates of unassigned residues of IRF-7 were estimated by standard interpolation methods and the final model following energy minimization was constructed employing the Discover module of Insight II (Accelrys). This model of the IRF-7 IAD is illustrated in Fig. 5B that shows all the protein secondary features of this component inclusive of the H3/H4 α -helices of the ID and the H5 α -helix of the C-terminal SRD.

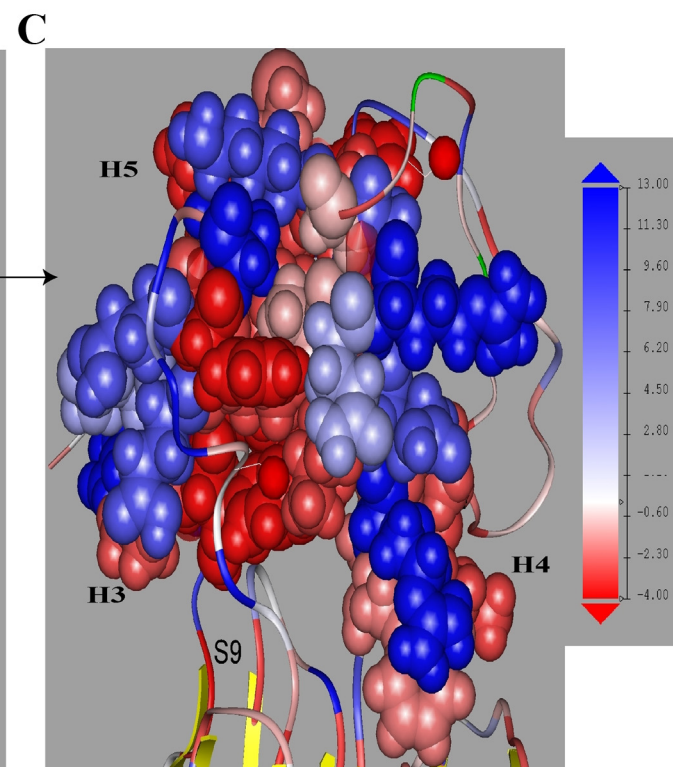
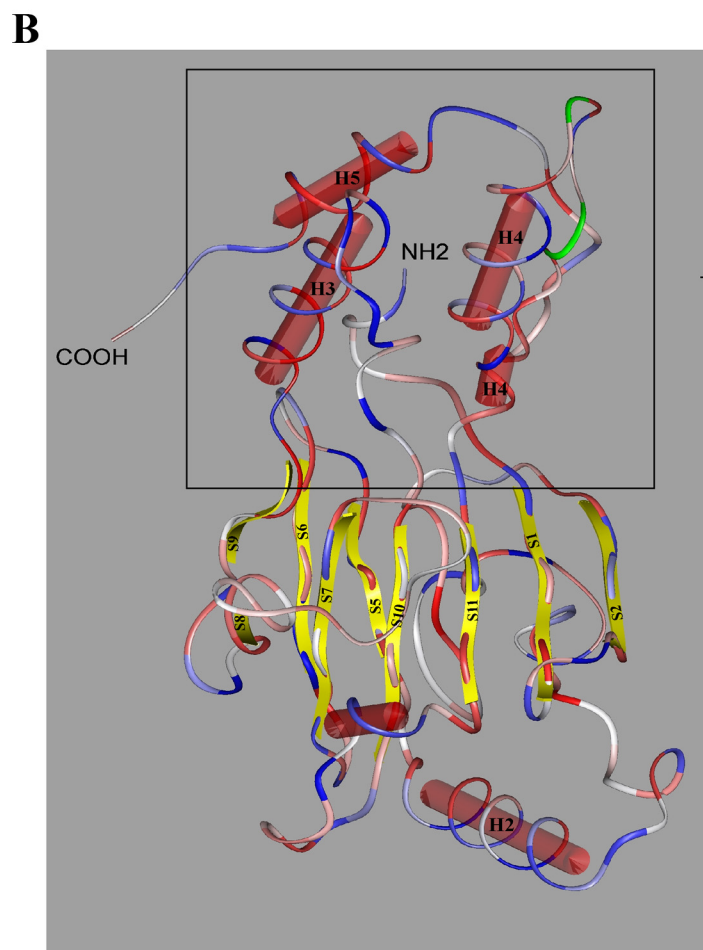
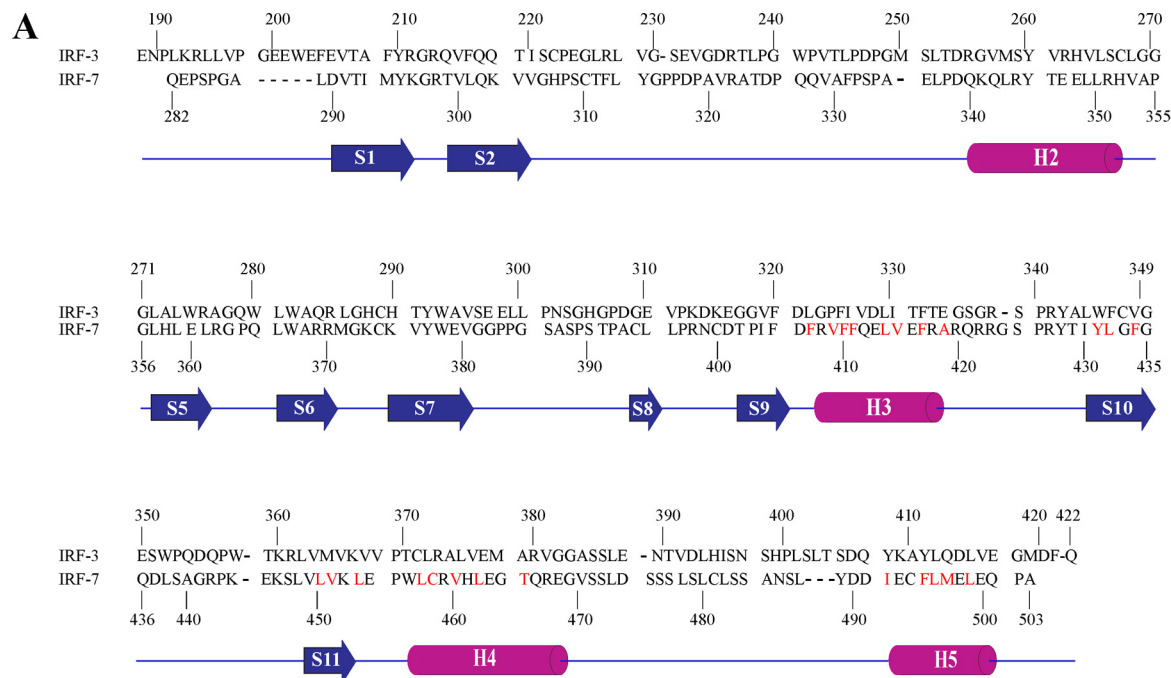
A space-filling model of the region spanning the H3-H4-H5 α -helices, as illustrated in Fig. 5C, clearly shows the increased hydrophobicity of this region along with the physical interactions among the H3, H4, and H5 α -helices mediated through hydrophobic contacts. A space filling model of the above region in 2 different orientations (with each helix represented in a distinct color), which further corroborates the interaction of the α -helices (H3 and H4) with the H5 helix is illustrated in supplemental Fig. S1. In addition to its interaction with the H5 α -helix, from our modeling data we also predict that the apparently exposed hydrophobic region spanning the H3-H4 α -helices (Fig. 5C) could also be involved in associating with regions closer to the N terminus of IRF-7 (data not shown). Taken together our molecular modeling approaches provide a model for the maintenance of IRF-7 in a closed state conformation through interactions pivotally mediated by hydrophobic amino acid stretches spanning the H3 and H4 α -helices of the ID.

As the above modeling data were based on computer-generated images, we did feel compelled to verify the predicted closed state IRF-7 model and to gain more details about the structure through experimental approaches. Toward this, we employed a systematic protein mapping approach. Employing the Y2H assay, we attempted to investigate the interaction patterns of the different domains of IRF-7 with its ID. The different IRF-7 exons (numbering 1–10 from the N to the C terminus encompassing the different domains of IRF-7; Fig. 6) constituting the prey along with the bait (IRF-7 ID segment spanning aa 283–466) were simultaneously co-transformed into yeast cells. Interacting prey-bait pairs were then identified through selection of *His*⁺*LacZ*⁺ yeast transformants as earlier described on plates incorporated with increasing concentrations of 3-AT but lacking histidine. Fig. 6A illustrates the *HIS3/LacZ* phenotypes of yeast colonies transformed with the respective prey-bait pairs. Herein, the (i) *HIS3* phenotype is shown as indicated by growth of these yeast colonies on plates lacking histidine incorporated with 50 mM 3-AT and (ii) *LacZ* phenotype is represented as indicated by findings of the β -galactosidase performed on the colonies. Taken together, the Y2H findings indicated interactions of both the N-terminal (exons 1/2 and 3) and C-terminal (exon 10) exons

Mechanisms of Inhibition of IRF-7

with the IRF-7 ID, represented schematically in Fig. 6B. Interestingly the ID interacting region, the N-terminal exons (amino acids 1–131), and the C-terminal exon (amino acids 452–503) span the N-terminal DBD and the C-terminal SRD

of IRF-7, respectively (Fig. 6B). Thus the contact established by ID with both the C and N terminus leads to a closed conformation structure wherein the IRF-7 functional domains including the C-terminal SRD and the N-terminal DBD and



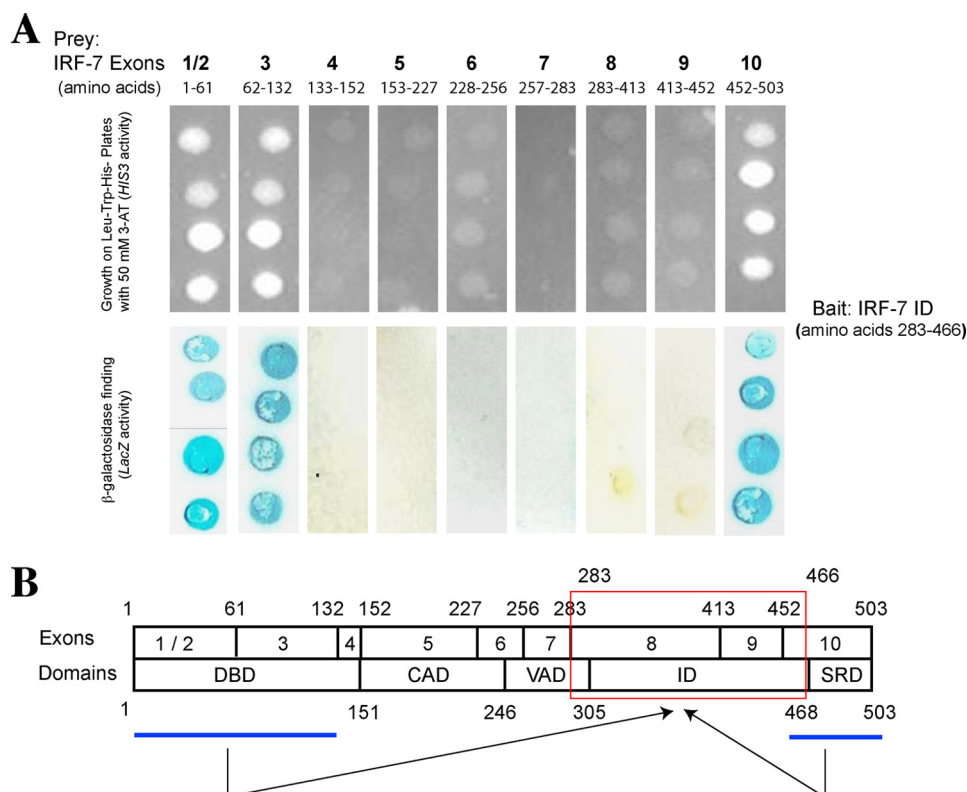


FIGURE 6. Interaction patterns of IRF-7 exons with the IRF-7 ID. *A*, the different IRF-7 exons (prey) cloned into the pACT2 vector were tested for their abilities to interact with the bait IRF-7 ID (aa 283–466) by a standard yeast two-hybrid (Y2H) assay. Yeast transformants positive for the prey-bait interaction were first selected on plates lacking leucine, tryptophan, and histidine (incorporated with 50 mM 3-AT, taken as the cut-off point) and subsequently assayed for β -galactosidase activity by a standard colony filter assay. The *upper panel* shows the growth patterns of prey-bait transformed yeast colonies on plates lacking histidine (with 50 mM 3-AT) as an indicator of *HIS3* activity. The *lower panel* exhibits the β -galactosidase assay findings on these transformed yeast colonies as an indicator of *LacZ* activity. *B*, schematic representation of the interaction patterns of the different IRF-7 exons with the IRF-7 ID. The different IRF-7 exons (1–10) are shown schematically (*upper panel*) with the numbers indicating the corresponding amino acid positions of the respective exons. Findings of the above Y2H assay revealed the interaction of both the N-terminal (exons 1/2 and 3) and C-terminal (exon 10) exons (indicated by dark blue lines) with the IRF-7 ID (enclosed within the red bordered rectangle). The *lower panel* represents a schematic representation of the different domains of IRF-7, including the DBD, CAD, VAD, ID, and SRD. Extrapolation from the IRF-7 exon interaction pattern is also indicated in the *lower panel*, wherein both the N-terminal DBD and C-terminal SRD (indicated by blue lines underneath) interact with the IRF-7 ID (indicated within the red bordered rectangle).

the CAD tend to be masked thereby locking the IRF-7 molecule in an inactive/folded state.

Serine moieties in the C-terminal SRD of IRF-7 (23, 24) serve as target substrates toward IRF-7 phosphorylation, which constitutes the initial step in its activation. Our modeling approach also predicted that through interactions mediated by the ID, a cluster of target serine residues at aa positions 475, 476, 477, 479, and 487 are likely to be buried in the closed/latent state conformation of IRF-7 making them less amenable to phosphorylation (supplemental Fig. S2). Viral invasion of a cell prompts the virus-mediated kinases IKK and TBK1 (38, 39) to bring about the addition of negatively charged phosphate groups to the serine moieties (23, 24). The associated charge repulsions brought about by this could re-

sult in a significant perturbation in the closed conformation of IRF-7 mediated by the ID. Similar to IRF-3, this could culminate in the conversion of IRF-7 to an open conformation wherein all the functional domains of IRF-7 are exposed resulting in initiation of subsequent downstream activation.

Significance of the Hydrophobic Region Spanning the H3–H4 α -Helices in IRF-7 Activation—The above described model had suggested candidate regions within the IRF-7 ID (stretch spanning the H3–H4 helices) having the potential to play a central role in autoinhibition of IRF-7 in the latent state. To verify the role of this region including the two helices and the sequence between them, we constructed a series of deletion mutants in the ID of IRF-7 (designated as mutants ID10–ID20, Fig. 7A) across the entire length of the ORF45

FIGURE 5. Predicted structure of the IRF-7 IAD segment. *A*, sequence alignment of the IRF-3 and IRF-7 IAD. Primary amino acid sequence alignment of the IRF-3 and IRF-7 IAD. The predicted secondary structures of IRF-7 are shown below the alignment with H representing the α -helices and S representing the β sheets. Hydrophobic amino acids in the IRF-7 sequences are indicated in red. The numbers alongside the sequences represent the respective amino acid positions. *B*, predicted structure of the IRF-7 IAD segment. The x-ray crystal structure of IRF-3 (PDB 1J2F) was obtained from the Protein Data Bank at the Research Collaboratory for Structural Bioinformatics. The C-terminal section of the B chain (residues 189–422) served as the structure template. The sequence of IRF-7 (residues 281–503) was aligned to the IRF-3 structure by sequence similarity, and the coordinates of homologous amino acids were transferred from IRF-3 to IRF-7 using the Homology module of Insight II (Accelrys). The coordinates of unassigned residues of IRF-7 were estimated by standard interpolation methods with the final predicted structure energy minimized using the Discover module of Insight II. The region spanning the H3–H4–H5 α -helices (within the boxed square) is illustrated in *C* as a space-filling model clearly showing the physical interaction of the three helices along with the increased hydrophobicity of this region. The hydrophobicity scale index (25) is shown alongside the *right panel* with hydrophobicity increasing from top to the bottom of the scale.

Mechanisms of Inhibition of IRF-7

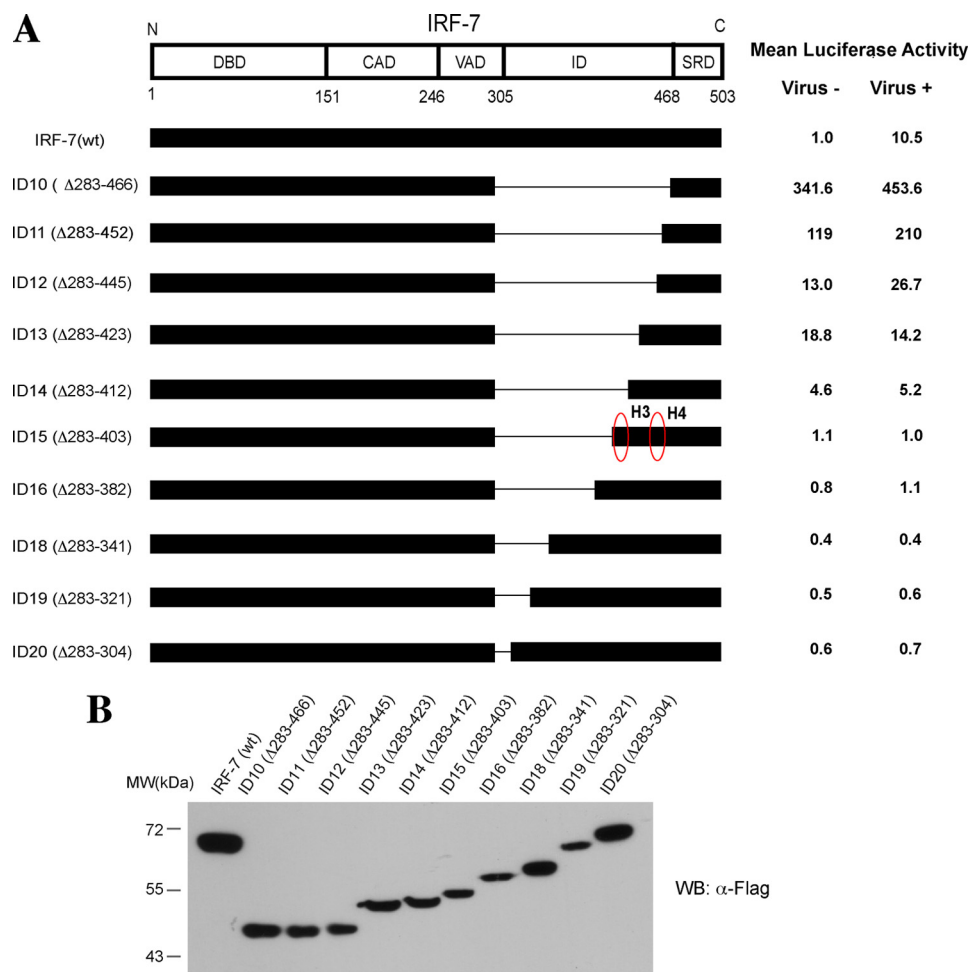


FIGURE 7. Deletions of the hydrophobic amino acid-rich IRF-7 ID region spanning H3–H4 α -helices results in increased transcription of the IFNA1 promoter. *A*, a series of progressive deletions in the ID of IRF-7 (designated as mutants ID10–ID20) across the entire length of the ORF45-binding region was generated and cloned into a pCMV-FLAG vector. Reporter plasmids containing the firefly luciferase gene under control of the human IFNA1 promoter were co-transfected into subconfluent monolayers of HEK 293T cells along with either the wild-type (WT) IRF-7 or the progressive deletion mutants (ID10–ID20). pRL-TK reporter plasmid encoding the *Renilla* luciferase (*Ren*) was included as an internal control. At 8 h post-transfection, cells were either left uninfected or infected with Sendai virus. Cells were lysed and the luciferase (*Luc*) activities measured at 24 h post-infection and represented relative to the *Ren* internal control gene. The mean luciferase activity with respect to transcription of the IFNA1 promoter either in the absence or presence of virus is indicated on the left. The red bordered circles represent localization of the H3 and H4 α -helices in the IRF-7 ID. The upper panel depicts a schematic representation of the domain structure of IRF-7 with the DBD, CAD, VAD, ID, and SRD. *B*, the expression of these mutants in HEK 293T cells was analyzed by a Western blot (WB) using an anti-FLAG antibody. This was performed to check for both the presence of expression and comparable levels of expression of these mutant plasmids.

binding region (spanning aa 283–466). This approach allowed us to conveniently and reliably assess the function of different domains in this region. Given that the IRF-7 ID is a very sensitive domain such that any small deletions in the ID rendered the molecule inactive, but removal of the entire domain (Δ 283–466) led to a constitutive hyperactive form, we analyzed the ID region by starting with deletion mutant ID10 (with deletion of the entire stretch of the ID from aa 283–466) and gradually added small amino acid fragments back to the molecule. These mutants were examined for their ability to activate the IFNA1 promoter in the absence and presence of Sendai virus.

The IRF-7 deletion mutant ID10 (with a deletion of aa 283–466) displayed a constitutive activity that activated the IFNA1 promoter at a level of 342-fold higher than that of wild-type (WT) IRF-7 in uninfected cells and at a 43-fold higher level than WT IRF-7 in virally infected cells, respectively (Fig. 7A). Then, amino acids were gradually added back to deletion mu-

tant ID10 from the C-terminal direction. As shown in Fig. 7A, an addition of 14 amino acids to the C terminus (the mutant ID11 with a deletion of aa 283–452), which adds the H4 helix to the molecule, still maintained the constitutive hyperactivity of IRF-7 although there was greater than 50% reduction of the IFNA1 promoter transcription (Fig. 7A). Addition of seven more amino acids to the C terminus (the mutant ID12 with a deletion of aa 283–445), which adds the S11 β -sheet to the molecule, resulted in an 8-fold drop in activation of the IFNA1 promoter. Further sequential additions of amino acids led to proportionate decreases in transcription of the IFNA1 promoter until it reached almost undetectable levels following addition of amino acids at the C terminus until 403 (the mutant ID15 with a deletion of aa 283–403), beyond which any further amino acid addition had no discernible effect (Fig. 7A). Such similar effects on the transcription activity of the IFNB promoter was also witnessed with these IRF-7 ID deletion mutants (data not shown). Thus, these interesting obser-

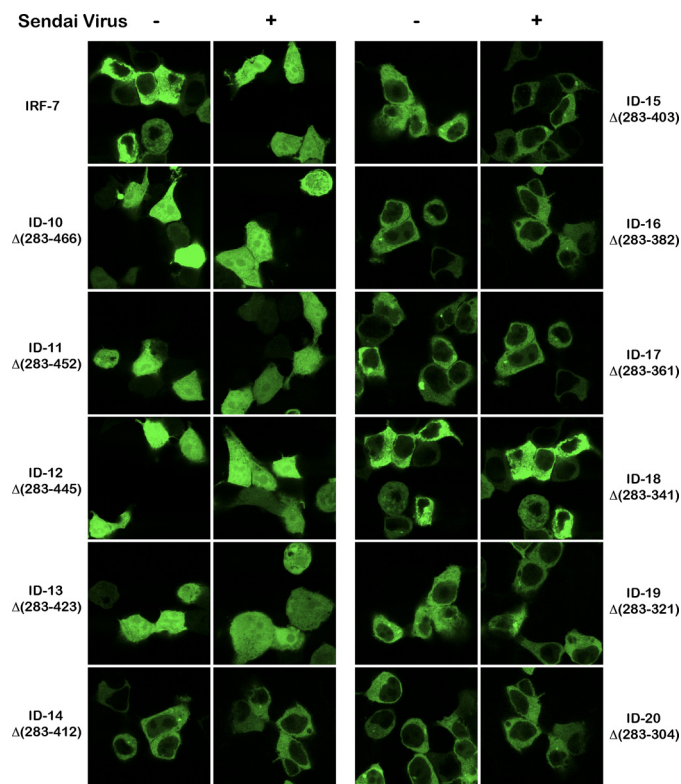


FIGURE 8. Deletions of the hydrophobic amino acid-rich IRF-7 ID region spanning H3–H4 α -helices results in nuclear translocation of IRF-7. A set of progressive IRF-7 ID deletion mutants (ID10–ID20) as well as the wild type IRF-7 cloned into an EGFP-tagged vector were individually transfected into HEK 293T cells grown on coverslips. The transfected cells were challenged with Sendai virus 16 h post-transfection. Twelve hours post-infection, both the uninfected (–) and virus-infected (+) cells were washed with PBS and subsequently fixed. The coverslips were mounted onto slides and examined under a confocal microscope (Nikon) for the intracellular localization patterns of the transfected IRF-7 expressing plasmids.

observations suggest that a gradual addition of the region encompassing the H3–H4 α -helices of the IRF-7 ID, spanning aa 407–466, likely brings about a closed conformation of IRF-7 (through hydrophobic interactions) mimicking the latent stage. Thus in the absence of any viral infection, the above region is able to pack IRF-7 into a closed tight structure that likely prevents any further activation of IRF-7.

Nuclear translocation is a hallmark of the IRF-7 activation following virus infection. Thus, to further confirm the role of the region spanning H3–H4 α -helices in IRF-7 activation, we examined the effects of the above mentioned deletion mutations spanning the ID region of IRF-7 (mutants ID10–ID20) on the nuclear translocation of the IRF-7 protein. The full-length IRF-7 and the deletion mutants as above were individually cloned in the pEGFP-C3 vector and expressed as GFP-tagged proteins in HEK 293T monolayer cells grown on coverslips. A set of transfected cells were challenged with Sendai virus 16 h post-transfection and another set left untreated. Cells were visualized under a confocal microscope 12 h post-infection along with the mock infected cells. In the absence of viral invasion, wild type IRF-7 was totally localized to the cytoplasm but exhibited a more nuclear translocation following virus challenge as evidenced by a uniform fluorescence throughout the cell (Fig. 8). The deletion mutant ID10 (Δ 283–

466) with complete deletion of the ID revealed a nuclear translocation regardless of Sendai virus challenge (Fig. 8). Mutants exhibiting partial deletions of the hydrophobic amino acid-rich region spanning the H3–H4 α -helices of the ID (the mutants ID11–ID13) also exhibited a nuclear translocation as shown in Fig. 8. These observations could thus explain the increased constitutive transcription of the IFNA1 promoter observed with these mutants in the earlier luciferase reporter assay (Fig. 7).

Nuclear translocation of IRFs has been shown to be brought about by specific nuclear localization sequences (NLS). These occur either as traditional basic amino acid-rich bipartite or monopartite sequences localized to the N terminus as seen with IRFs-1, -2, -4, -5, and -9, respectively (32, 40, 41). IRF-3 has a NLS characterized by the presence of just 2 basic amino acid residues in its N terminus with functional capability (42). In IRF-7 also, putative NLS have been shown to be present in the N-terminal region spanning aa 1–246 (23). The possible association of the apparently exposed hydrophobic region spanning the H3–H4 α -helices with regions closer to the N terminus of IRF-7 earlier suggested by our model could well result in effectual burial of the NLS of IRF-7 in the absence of viral signals, but the same can be unmasked by a viral signal-induced conformation change resulting in nuclear translocation as seen with the wild type IRF-7 following Sendai virus infection (Fig. 8). Interestingly nuclear translocation of IRF-7 ID deletion mutants ID10–ID13, even in the absence of viral infection (Fig. 8), also suggests a similar unmasking of the NLS consequent to the absence of a closed state IRF-7 conformation following deletion of the hydrophobic amino acid-rich region of the ID spanning the H3–H4 α -helices.

The deletion mutants possessing the hydrophobic amino acid-rich stretch spanning the ID (mutants ID14–ID20) failed to localize to the nucleus regardless of the presence of a viral signal (Fig. 8). This result is consistent with the effects of these mutations on IRF-7-dependent transcription of the IFNA1 promoter seen earlier (Fig. 7), thereby pointing to the generation of a closed state IRF-7 conformation consequent to the presence of the hydrophobic region spanning the H3–H4 α -helices. Interestingly these findings also suggest that the entire ID (aa 283–466) may function as a hinge that controls movement of the molecule during the switch between the latent and active conformation. Any damage or deletion of the region even adjacent to the H3–H4 domains (aa 283–406) may affect the function of the hinge, *i.e.* the movement of the molecule, thereby resulting in a dead-locked inactive form of IRF-7. However, if the entire “hinge” (ID) is removed, the molecule becomes an unclosed molecule with constitutive activities.

Thus in this study by employing a combination of molecular modeling and *in vitro* based approaches we have been able to gain valuable insights into the IRF-7 ID, a crucial component controlling the switch of IRF-7 from a folded inactive state to an open active conformation. Interestingly with the crystal structure of IRF-7 N-terminal DBD recently being described (43), the only segment of IRF-7 about which little structural information is known is a region in the middle

Mechanisms of Inhibition of IRF-7

spanning ~150 amino acids primarily constituted by the CAD. Although in this study we were primarily interested in the IRF-7 ID due to its KSHV ORF45 binding capacity, futuristic structural information on the CAD component would definitely help to completely understand the IRF-7 structure.

Hypothesized Model for ORF45-mediated Inhibition of IRF-7 Activation—We had earlier shown that KSHV ORF45 interacts with IRF-7 inhibiting both its phosphorylation and nuclear translocation (21). A detailed mechanism underlying these processes has, however, remained elusive, which we were motivated to comprehend. Our study finding identified the ORF45 binding domain on IRF-7 to its ID, the region shown in this study to critically control the switch between the closed/inactive and opened/active forms of IRF-7. Thus based on these concrete observations, we hypothesize a very feasible and rational model, wherein KSHV ORF45 by binding to the ID of IRF-7 maintains the molecule in an inactive/labile state. This action of ORF45 likely prevents the entire cascade of downstream IRF-7 activation steps inclusive of the ensuing virus-induced phosphorylation and its nuclear translocation (21), critical for transcription of the type I IFN genes.

REFERENCES

1. Levy, D. E., Marié, I., Smith, E., and Prakash, A. (2002) *J. Interferon Cytokine Res.* **22**, 87–93
2. Nguyen, H., Hiscott, J., and Pitha, P. M. (1997) *Cytokine Growth Factor Rev.* **8**, 293–312
3. Solis, M., Goubau, D., Romieu-Mourez, R., Genin, P., Civas, A., and Hiscott, J. (2006) *Biochem. Pharmacol.* **72**, 1469–1476
4. Zhang, L., and Pagano, J. S. (2002) *J. Interferon Cytokine Res.* **22**, 95–101
5. Sato, M., Suemori, H., Hata, N., Asagiri, M., Ogasawara, K., Nakao, K., Nakaya, T., Katsuki, M., Noguchi, S., Tanaka, N., and Taniguchi, T. (2000) *Immunity* **13**, 539–548
6. Marié, I., Durbin, J. E., and Levy, D. E. (1998) *EMBO J.* **17**, 6660–6669
7. Sato, M., Hata, N., Asagiri, M., Nakaya, T., Taniguchi, T., and Tanaka, N. (1998) *FEBS Lett.* **441**, 106–110
8. Sadler, A. J., and Williams, B. R. (2008) *Nat. Rev. Immunol.* **8**, 559–568
9. Der, S. D., Zhou, A., Williams, B. R., and Silverman, R. H. (1998) *Proc. Natl. Acad. Sci. U.S.A.* **95**, 15623–15628
10. Honda, K., Yanai, H., Negishi, H., Asagiri, M., Sato, M., Mizutani, T., Shimada, N., Ohba, Y., Takaoka, A., Yoshida, N., and Taniguchi, T. (2005) *Nature* **434**, 772–777
11. Honda, K., Yanai, H., Takaoka, A., and Taniguchi, T. (2005) *Int. Immunology* **17**, 1367–1378
12. Honda, K., and Taniguchi, T. (2006) *Nat. Rev. Immunol.* **6**, 644–658
13. Honda, K., Yanai, H., Mizutani, T., Negishi, H., Shimada, N., Suzuki, N., Ohba, Y., Takaoka, A., Yeh, W. C., and Taniguchi, T. (2004) *Proc. Natl. Acad. Sci. U.S.A.* **101**, 15416–15421
14. Wu, L., Fossum, E., Joo, C. H., Inn, K. S., Shin, Y. C., Johannsen, E., Hutt-Fletcher, L. M., Hass, J., and Jung, J. U. (2009) *J. Virol.* **83**, 1140–1146
15. Joo, C. H., Shin, Y. C., Gack, M., Wu, L., Levy, D., and Jung, J. U. (2007) *J. Virol.* **81**, 8282–8292
16. Yu, Y., Wang, S. E., and Hayward, G. S. (2005) *Immunity* **22**, 59–70
17. Lin, R., Noyce, R. S., Collins, S. E., Everett, R. D., and Mossman, K. L. (2004) *J. Virol.* **78**, 1675–1684
18. Hahn, A. M., Huye, L. E., Ning, S., Webster-Cyriaque, J., and Pagano, J. S. (2005) *J. Virol.* **79**, 10040–10052
19. Zhu, F. X., and Yuan, Y. (2003) *J. Virol.* **77**, 4221–4230
20. Zhu, F. X., Cusano, T., and Yuan, Y. (1999) *J. Virol.* **73**, 5556–5567
21. Zhu, F. X., King, S. M., Smith, E. J., Levy, D. E., and Yuan, Y. (2002) *Proc. Natl. Acad. Sci. U.S.A.* **99**, 5573–5578
22. Zhu, F. X., Sathish, N., and Yuan, Y. (2010) *PLoS One* **5**, e10573
23. Lin, R., Mamane, Y., and Hiscott, J. (2000) *J. Biol. Chem.* **275**, 34320–34327
24. Marié, I., Smith, E., Prakash, A., and Levy, D. E. (2000) *Mol. Cell. Biol.* **20**, 8803–8814
25. Engelman, D. M., and Steitz, T. A. (1981) *Cell* **23**, 411–422
26. Servant, M. J., Tenoever, B., and Lin, R. (2002) *J. Interferon Cytokine Res.* **22**, 49–58
27. Lin, R., Heylbroeck, C., Pitha, P. M., and Hiscott, J. (1998) *Mol. Cell. Biol.* **18**, 2986–2996
28. Lin, R., Mamane, Y., and Hiscott, J. (1999) *Mol. Cell Biol.* **19**, 2465–2474
29. Qin, B. Y., Liu, C., Lam, S. S., Srinath, H., Delston, R., Correia, J. J., Derynck, R., and Lin, K. (2003) *Nat. Struct. Biol.* **10**, 913–921
30. Eisenbeis, C. F., Singh, H., and Storb, U. (1995) *Genes Dev.* **9**, 1377–1387
31. Brass, A. L., Kehrl, E., Eisenbeis, C. F., Storb, U., and Singh, H. (1996) *Genes Dev.* **10**, 2335–2347
32. Barnes, B. J., Kellum, M. J., Field, A. E., and Pitha, P. M. (2002) *Mol. Cell. Biol.* **22**, 5721–5740
33. Rozen, R., Sathish, N., Li, Y., and Yuan, Y. (2008) *J. Virol.* **82**, 4742–4750
34. Takahasi, K., Suzuki, N. N., Horiuchi, M., Mori, M., Suhara, W., Okabe, Y., Fukuhara, Y., Terasawa, H., Akira, S., Fujita, T., and Inagaki, F. (2003) *Nat. Struct. Biol.* **10**, 922–927
35. Needleman, S. B., and Wunsch, C. D. (1970) *J. Mol. Biol.* **48**, 443–453
36. Smith, T. F., and Waterman, M. S. (1981) *Adv. Appl. Math.* **2**, 482–489
37. Kabsch, W., and Sander, C. (1983) *Biopolymers* **22**, 2577–2637
38. Sharma, S., tenOever, B. R., Grandvaux, N., Zhou, G. P., Lin, R., and Hiscott, J. (2003) *Science* **300**, 1148–1151
39. Fitzgerald, K. A., McWhirter, S. M., Faia, K. L., Rowe, D. C., Latz, E., Golenbock, D. T., Coyle, A. J., Liao, S. M., and Maniatis, T. (2003) *Nat. Immunol.* **4**, 491–496
40. Schaper, F., Kirchhoff, S., Posern, G., Köster, M., Oumard, A., Sharf, R., Levi, B. Z., and Hauser, H. (1998) *Biochem. J.* **335**, 147–157
41. Lau, J. F., Parisien, J. P., and Horvath, C. M. (2000) *Proc. Natl. Acad. Sci. U.S.A.* **97**, 7278–7283
42. Kumar, K. P., McBride, K. M., Weaver, B. K., Dingwall, C., and Reich, N. C. (2000) *Mol. Cell Biol.* **20**, 4159–4168
43. Panne, D., Maniatis, T., and Harrison, S. C. (2007) *Cell* **129**, 1111–1123